KF Post-Deposition Treatment of Industrial Cu(In,Ga)(S,Se)$_2$ Thin-Film Surfaces: Modifying the Chemical and Electronic Structure

Michelle Mezher [1,], Lorelle M. Mansfield [2], Kimberly Horsley [1,‡], Monika Blum [1], Robert Wieting [3], Lothar Weinhardt[1,4,5], Kannan Ramanathan [3], and Clemens Heske [1,4,5,]**

[1] Department of Chemistry and Biochemistry, University of Nevada, Las Vegas (UNLV), Las Vegas, NV 89154-4003, USA

[2] National Renewable Energy Laboratory (NREL), 15013 Denver West Parkway, Golden, CO 80401, USA

[3] STION, 6321 San Ignacio Avenue, San Jose, CA 95119, USA

[4] Institute for Photon Science and Synchrotron Radiation (IPS), Karlsruhe Institute of Technology (KIT), 76344 Eggenstein-Leopoldshafen, Germany

[5] Institute for Chemical Technology and Polymer Chemistry (ITCP), Karlsruhe Institute of Technology (KIT), 76128 Karlsruhe, Germany

[‡] New address: Hawaii Natural Energy Institute (HNEI), University of Hawaii at Manoa, 1680 East-West Rd, POST 109, Honolulu, HI 96822, USA

Corresponding Authors:

Michelle Mezher (mezherm@unlv.nevada.edu) and Clemens Heske (heske@unlv.nevada.edu)

ABSTRACT

The chemical and electronic structure of industrial chalcopyrite photovoltaic absorbers after KF post-deposition treatment (KF-PDT) is investigated using electron spectroscopies to probe the occupied and unoccupied electronic states. In contrast to a variety of recent publications on the impact of KF-PDT, this study focuses on *industrial* $Cu(In,Ga)(S,Se)_2$ absorbers that also contain sulfur at the surface. We find that the KF-PDT removes surface adsorbates and oxides, and also observe a change in the S/Se ratio. Furthermore, the KF-PDT leads to a Cu reduction at the surface, but to a much lower degree than the strongly Cu-depleted or even Cu-free surfaces reported for (non-industrial) sulfur-free $Cu(In,Ga)Se_2$ absorbers. The valence band maximum at the surface is found at a lower energy compared to the untreated absorber, and the conduction band minimum is found at a higher energy, overall revealing a widening of the band gap in the surface region.

MAIN TEXT

In November 2014, a new world record for $Cu(In,Ga)Se_2$ (CIGSe) thin-film photovoltaics with a flexible substrate was set by Empa, raising the energy conversion efficiency from 18.7% to 20.4%.[1] The large jump in conversion efficiency was achieved with an alkali post-deposition treatment (PDT) and attributed to its impact on the CdS/CIGSe interface as well as the reduction of optical losses in the CdS buffer layer.[1] With this new record, KF treatments have become a "hot topic" in the chalcopyrite research community. Only one year later, ZSW achieved a world record of 21.7% [2] using PDT (and a soda lime glass substrate). Most recently, a new ZSW record system (22.6%) employed a PDT treatment using heavy alkali atoms.[3]

While the importance of Na incorporation into the CIGSe absorber is well known and established,[4–7] widespread research into the effect of potassium in CIGSe has only emerged in the past few years.[1,3,8–17] A common finding with the KF-PDT is the depletion of Cu at the surface of the CIGSe absorber, which in turn affects the surface electronic structure; however, this has only been reported for CIGSe deposited using the three-stage coevaporation process commonly used to create laboratory-scale research devices.[1,10,18] Industrial companies, on the other hand, generally do not use the three-stage coevaporation process and in some cases also incorporate S into the chalcopyrite absorber.[19–21] To bridge the gap between laboratory scale and industrial module efficiencies, it is required to understand the role of KF in industrial chalcopyrites, especially to uncover and optimize the "hidden" parameters of the KF treatment. Thus, to gain insight on the effects of KF-PDT on industrial $Cu(In,Ga)(S,Se)_2$ (CIGSSe) surfaces, we determine its influence on the chemical and electronic surface properties of absorbers from Stion Corporation's manufacturing process using x-ray and UV photoelectron spectroscopy (XPS and UPS), x-ray excited Auger electron spectroscopy (XAES), and inverse photoemission spectroscopy (IPES).

Two CIGSSe absorbers from Stion were deposited using a proprietary 2-stage process. The first step involves physical vapor deposition of Cu, In, and Ga, while the second step involves the sulfurization and selenization of the metals to create the CIGSSe thin film absorber[20]. Typical absorber thicknesses are ~1-2 um. One of the absorbers was packaged as-is (called "untreated absorber"), while for the other absorber (called "KF-PDT absorber"), a KF-PDT was performed by evaporating KF and Se onto the absorber surface and annealing for 15 minutes at 330 °C. Subsequently, the sample was rinsed (100 ml H_2O + 12.5 mL 28% NH_4OH reagent) for four minutes at 65 °C. Completed twin KF-PDT devices exhibited efficiencies with an average of 13.8% and maximum of 14.1%.

The samples were briefly air-exposed, packed, and vacuum-sealed under dry nitrogen before being sent to UNLV. The samples were unsealed and mounted in an inert environment and introduced to the UHV system without any further air exposure. Mg and Al K_α irradiation and a SPECS PHOIBOS 150 MCD electron analyzer were employed for XPS and XAES measurements. He II excitation was used for the UPS measurements. IPES was performed using a commercial electron gun (Staib NEK 150-1) and a custom-built Dose-type iodine detector. The XPS and XAES spectra were calibrated using Auger and core-level peaks of clean Cu, Ag, and Au foils,[22] while UPS and IPES spectra were calibrated with the Fermi energy of a sputter-cleaned Au foil. The valence band maximum (VBM) and conduction band minimum (CBM) were determined by linear extrapolation of the leading edge in the valence band (UPS) and conduction band (IPES) spectra, respectively[23]. Detailed scans were used for all quantitative and semi-quantitative analyses of the samples in this study. The base pressure in the analysis chamber was below 5×10^{-10} mbar.

Figure 1 shows XPS survey spectra of the untreated absorber (black) and the KF-PDT absorber (red), taken with Mg K_α excitation (1253.6 eV). The pertinent CIGSSe photoemission

and Auger lines (Cu, In, Ga, Se, S) are labeled, as well as the lines associated with Na, C, and O (note that, for the untreated absorber, the O 1s peak is particularly pronounced). Due to the presence of this C- and O-containing surface adsorbate layer, all low-kinetic energy (high-

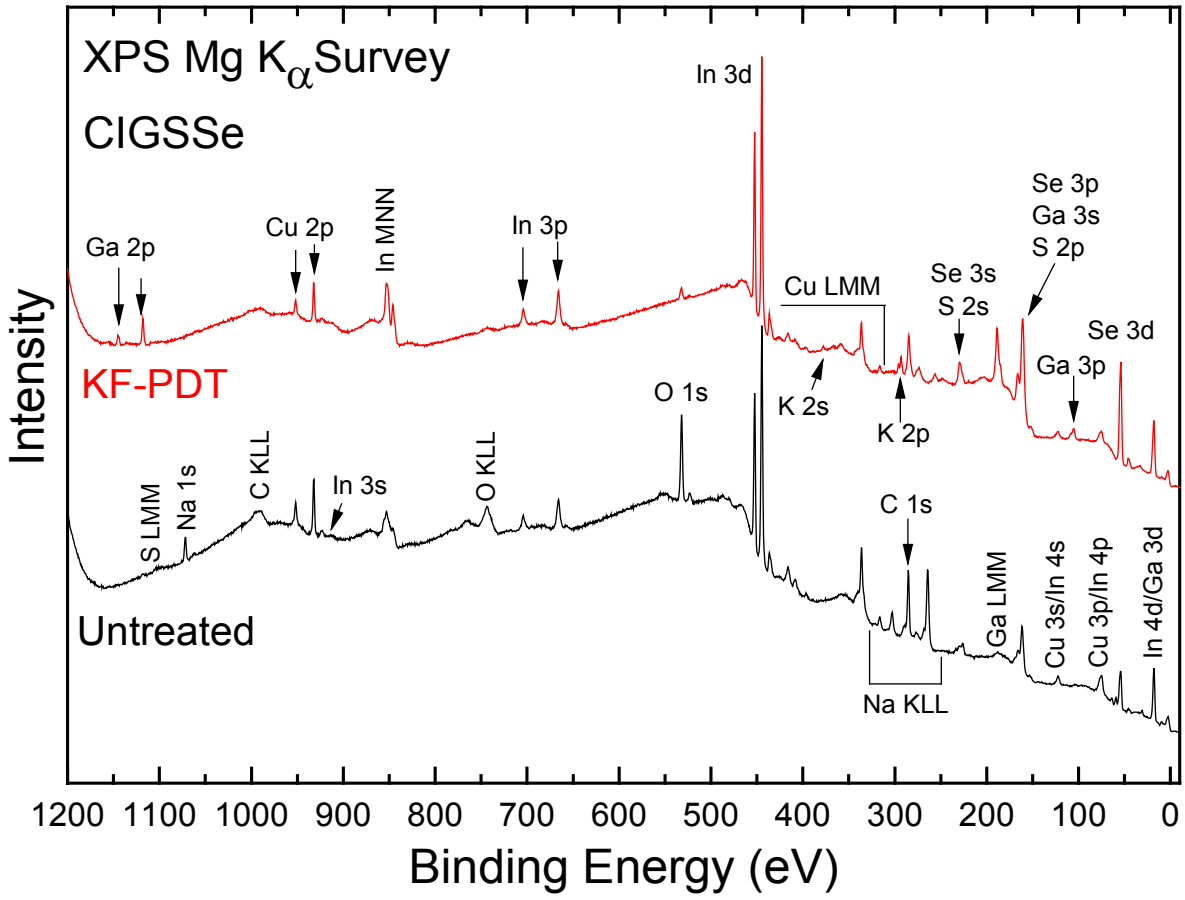

Figure 1: Mg K_α XPS survey spectra of a CIGSSe bare absorber before (black, "Untreated") and after (red, "KF-PDT") a KF post-deposition treatment.

binding energy) peaks in the survey spectrum (e.g., Ga 2p, Cu 2p, In MNN) are more strongly attenuated than those at higher kinetic energy (lower binding energy). For the KF-PDT absorber, the oxygen and carbon peaks are significantly reduced, indicating that the KF-PDT removes (a part of) the surface layer/adsorbates seen for the untreated absorber. The KF-PDT is also seen to remove Na from the surface. The intensities of the Ga and In peaks consequently increase after the KF-PDT. The Cu 2p peaks decrease slightly, in contrast to the behavior of the Ga and In peaks, but also in contrast to the much more pronounced Cu-depletion (or even removal)

reported in the literature for non-industrial and sulfur-free CIGSe.[1,8,9,11,13,16] Note that these absorbers are generally grown with a 3-stage process, which significantly differs from the 2-stage process employed here. Nevertheless, since the removal of adsorbates is expected to

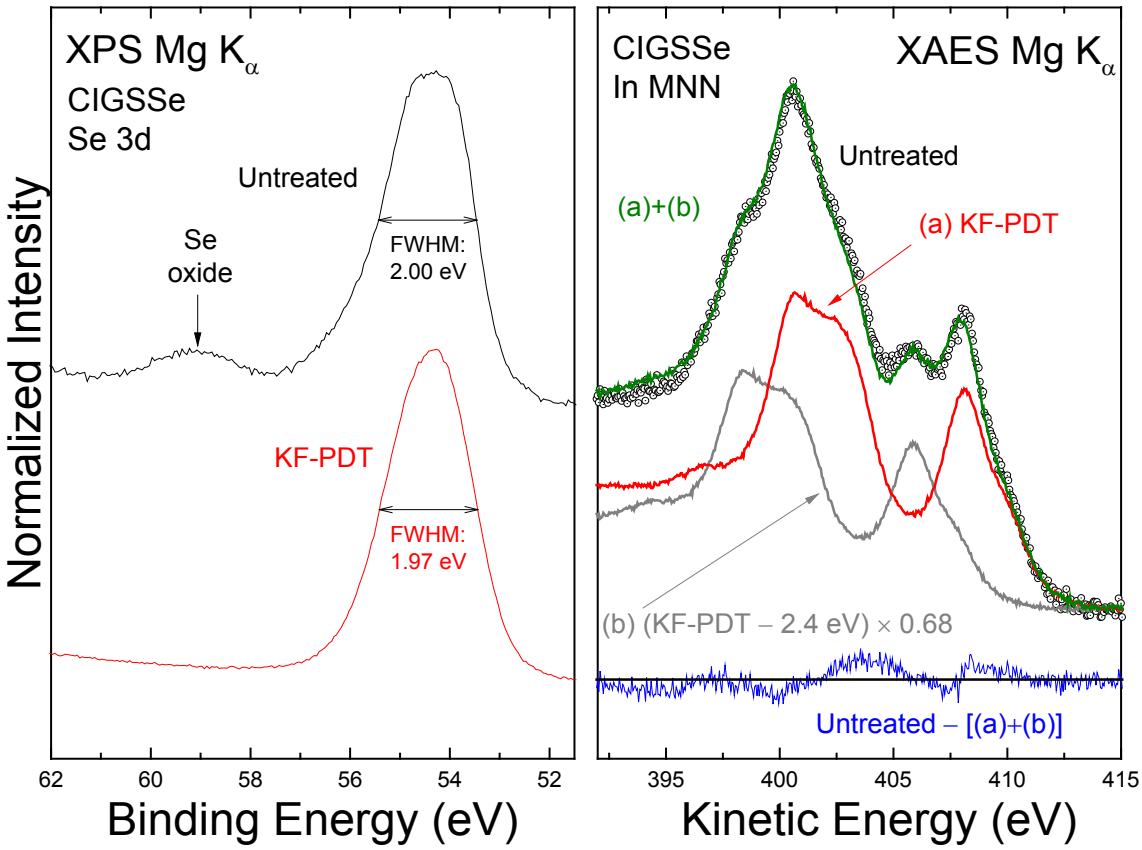

Figure 2. Mg K_α XPS and XAES detailed spectra of the Se 3d (left) and the In MNN (right) peaks of the absorber before (black line or circles) and after KF-PDT (red line). To describe the "Untreated" In MNN spectrum, a second (KF-PDT) In MNN spectrum, shifted by 2.4 eV to lower kinetic energy and multiplied by 0.68 (grey), is used to represent In-O contributions to the "Untreated" absorber. The sum of the shifted and unshifted KF-PDT spectra is shown in green, giving a good representation of the untreated sample (residual is shown in blue).

enhance all peak intensities of the underlying surface, the decreased Cu 2p signal indicates that indeed a significant amount of copper is removed from the surface by the KF-PDT. The KF-PDT also deposits K on the sample surface, as shown by the K 2s and 2p peaks. Note that the detail spectra of the F 1s region show no detectable trace of F (not shown).

In order to take a closer look at the effects of the KF-PDT on the CIGSSe absorber surface, detailed scans of the various Auger and photoemission lines were performed. As examples, Figure 2 shows detailed spectra of the Se 3d XPS peak (left) and the In MNN Auger peaks (right). In the Se 3d spectrum of the untreated absorber, a second component at 59 eV is indicative of Se oxide species. The KF-PDT removes the Se oxides and leads to a slight narrowing of the Se 3d peak and the removal of the shoulder on the high binding energy side (i.e., a slightly more uniform chemical environment of the selenide species). Likewise, oxide removal is also seen in the In MNN spectra. An indium oxide species is apparent for the untreated sample (black circles), as indicated by the additional spectral weight at ~406 eV and ~397 eV. [24] In the KF-PDT spectrum (red), this additional intensity is removed, leading to a dip at ~406 eV. To characterize the In MNN spectrum for the untreated absorber as a superposition of (at least) two indium species (most likely in an In-O and In-Se environment), the spectrum of the untreated absorber was fit with the KF-PDT spectrum (i.e., used as an In-Se reference) and a shifted and scaled "copy" of this spectrum to also reflect the In-O environment. The fit derives a relative intensity ratio of 1:0.68 (In-Se:In-O) and a shift of -2.4 eV for the oxide species. This shift leads to a kinetic energy of the In $M_4N_5N_5$ main peak of ~ 405 eV, in good agreement with tabulated values for various indium oxides (403.8 – 406.4 eV). [24,25] The residual shows that these two dominant species can describe the untreated absorber spectrum rather well.

With the KF-PDT, we also find a substantial change in the S/(S+Se) surface ratio, as seen in Figure 3. The Se 3s and S 2s region was fit utilizing Voigt functions, coupled Gaussian and Lorentzian widths, and a linear background using the Fityk Peak Fitting Program.[26] The quality of the fit is seen with the purple residual. Compared to the Se 3s main line (~ 229 eV), the untreated sample shows a higher sulfur (S 2s) intensity (~226 eV) than the KF-PDT sample. Also, a component at ~234 eV is found, indicative of a Se oxide (as also derived from the Se 3d spectrum above). We speculate that this component may also include contributions from S

oxides as well, and note that the oxide component is entirely removed after the KF-PDT (as in the case of the Se 3d oxide peak).

To compute the impact of the KF-PDT on the S/(S+Se) surface ratio, we follow three different approaches. First, we only take the non-oxide species into account and find that the

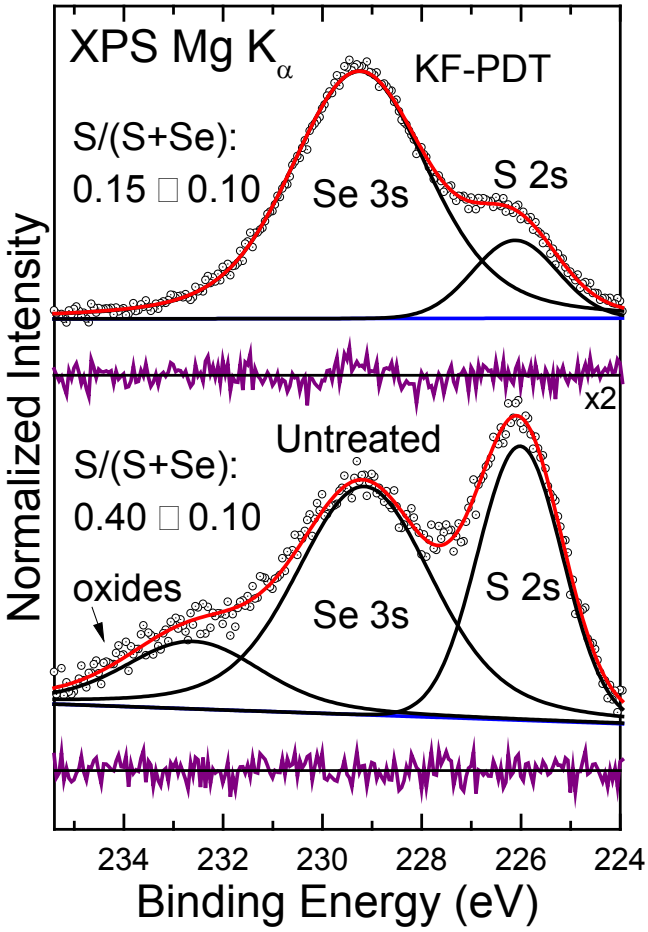

Figure 3. Mg K_α XPS detailed spectra of the Se 3s and S 2s peaks of the untreated (top) and KF-PDT (bottom) absorber. Data points are shown as black circles, fit components as solid black lines, the fit result in red, and the residual in purple.

S/(S+Se) surface ratio is reduced from 0.40 ± 0.10 (untreated) to 0.15 ± 0.10 (after KF-PDT). Second, we assume the extreme case that all of the oxide species is due to a selenium oxide and derive a S/(S+Se) surface ratio of 0.34 ± 0.10 for the untreated sample. Third, more mathematically involved, but the best estimate, we compute a selenium-oxide-to-selenide ratio of 0.06 from the Se 3d line. Ignoring a possible inelastic mean free path (IMFP) variation with kinetic energy between the Se 3d and 3s regions, we compute the selenium oxide contribution to

the “oxide” peak in Fig. 3 to be about 26%. Consequently, we assign 26% of the oxide peak area to selenium (oxide), and 74% to sulfur (oxide). The resulting S/(S+Se) surface ratio is 0.46 ± 0.10 for the untreated sample. In all cases, thus, we find a significant reduction of the sulfur surface concentration after KF-PDT.

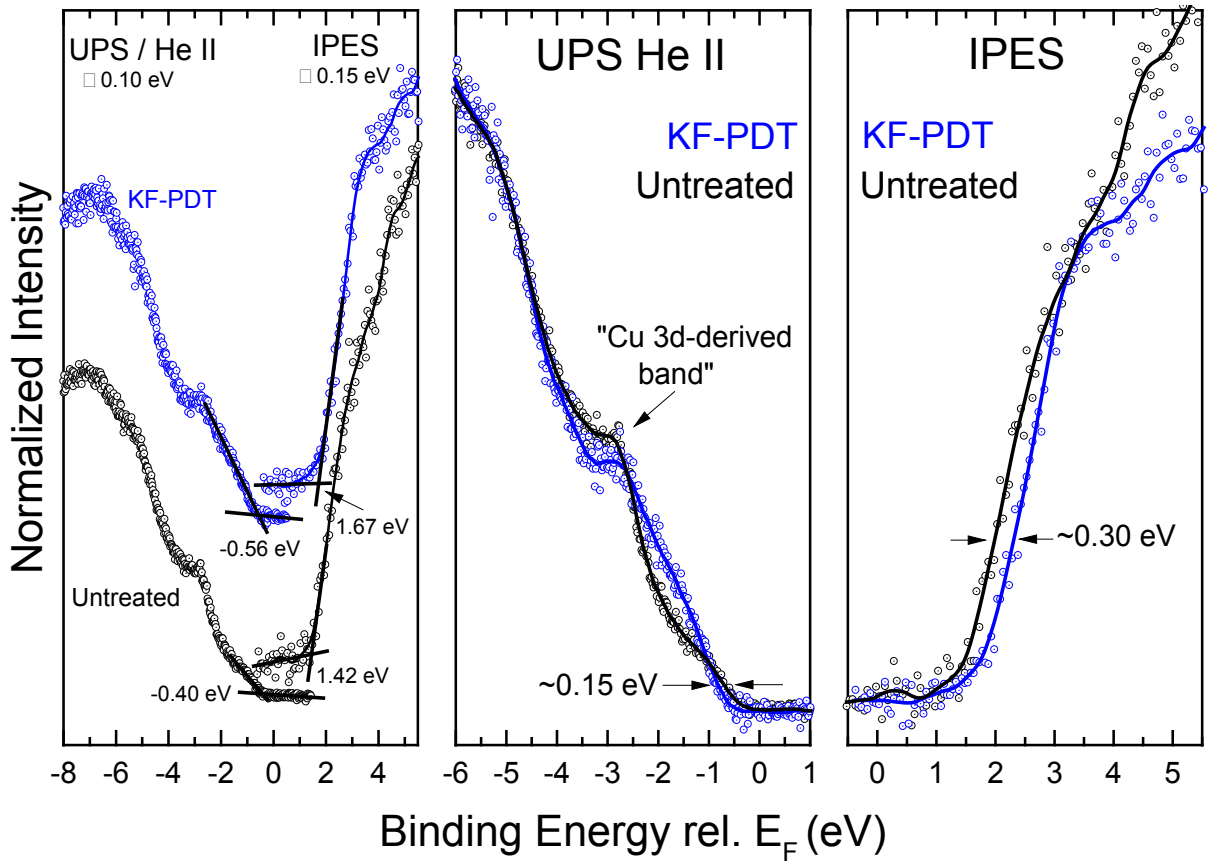

Figure 4. UPS and IPES spectra of the untreated CIGSSe absorber (black) and the KF-PDT CIGSSe absorber (blue). The left panel gives an overview of all spectra (IPES spectra were vertically shifted for clarity). The center panel shows the UPS spectra and the shift of the VBM (~0.15 eV), while the right panel shows the IPES spectra and the shift of the dominant CB edge (~0.3 eV).

In Figure 4 (left), He II UPS and IPES spectra are presented. They depict the valence band (UPS) and conduction band (IPES) of the untreated CIGSSe absorber (black) and the KF-PDT CIGSSe absorber (blue). We observe clear changes in both the valence and conduction band after the KF-PDT. The UPS spectra (enlarged in Fig. 4, center) show a clear change in spectral weight distribution and a downward shift of the VBM (by ~0.15 eV). The IPES spectra

(enlarged in Fig. 4, right) indicate an upward shift of the conduction band edge (by ~0.30 eV). Note that the surface "band gap" of the untreated absorber is dominated by the presence of oxides on the surface, and thus is larger than we normally find for "clean" CIGSSe absorber surfaces.

The *experimentally-derived* VBM and CBMs of the two absorbers are summarized in Scheme 1. The untreated CIGSSe absorber is shown in black on the left, while the KF-PDT CIGSSe absorber is shown in red on the right. In addition to the above-mentioned (significant) surface cleaning by the KF-PDT, we find that the electronic surface band gap obtained for the KF-PDT absorber is quite wide (2.23 ± 0.18 eV), even wider than that of the (adsorbate-covered) untreated absorber[27] and more similar to standard buffer layers. We thus speculate that the KF-PDT has several effects, especially for industrially relevant absorbers: first, the surface is "cleaned", and second the surface is chemically modified to potentially feature a wide-gap (i.e., optically less-absorbing) surface region (in our case also including a variation in the S/Se ratio and a reduction, but not full removal, of Cu atoms at the surface). Future work will be required to

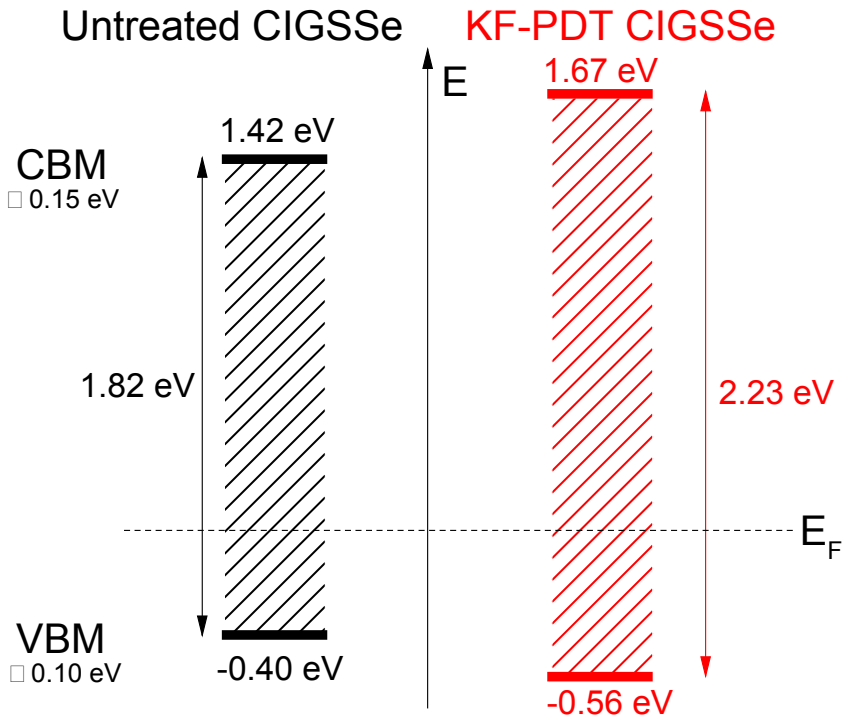

Scheme 1. VBM and CBM scheme of the untreated CIGSSe absorber (black, left) and the KF-PDT CIGSSe absorber (red, right). Band gap error bars are ±0.18 eV.

determine the extent (thickness) of the modified surface region and also study the CdS/KF-PDT CIGSSe interface and its band alignment, in particular in view of the possibility to optimize the band-bending at the absorber surface for optimal charge carrier separation.

To summarize, we note that KF-PDT has a significant impact on the electronic and chemical surface structure of industrial CIGSSe surfaces. Adsorbate peaks (associated with O and C), surface oxides (Se and In oxides), and surface Na species are removed during the KF-PDT. The K- PDT leads to a deposition of K, but we find no evidence for F on the surface of the treated sample. KF-PDT decreases the S/(S+Se) ratio and reduces the Cu content at the surface, both of which in turn influence the surface electronic properties. We find a spectral weight change near the VBM, a downward shift of the VBM, and upward shift of the CBM, revealing a widened surface band gap after KF-PDT. In total, thus, we find a significant number of KF-PDT-induced modifications of the CIGSSe surface, and further experiments will need to clarify which

of these modifications are primarily responsible for the improved conversion efficiency generally observed for KF-PDT-treated thin-film solar cell devices.

ACKNOWLEDGMENT

This work was funded by the U.S. Department of Energy (DOE) through the F-PACE Partnership (NREL subcontract No. ZEJ-2-22082-0.1).

REFERENCES

[1] A. Chirilă, P. Reinhard, F. Pianezzi, P. Bloesch, A.R. Uhl, C. Fella, L. Kranz, D. Keller, C. Gretener, H. Hagendorfer, D. Jaeger, R. Erni, S. Nishiwaki, S. Buecheler, and A.N. Tiwari, Nat. Mater. **12**, 1107 (2013).
[2] M.A. Green, K. Emery, Y. Hishikawa, W. Warta, and E.D. Dunlop, Prog. Photovolt. Res. Appl. **24**, 905 (2016).
[3] P. Jackson, R. Wuerz, D. Hariskos, E. Lotter, W. Witte, and M. Powalla, Phys. Status Solidi RRL – Rapid Res. Lett. **10**, 583 (2016).
[4] C. Heske, D. Eich, U. Groh, R. Fink, E. Umbach, T. van Buuren, C. Bostedt, N. Franco, L.. Terminello, M.. Grush, T.. Callcott, F.. Himpsel, D.. Ederer, R.C.. Perera, W. Riedl, and F. Karg, Thin Solid Films **361**–**362**, 360 (2000).
[5] C. Heske, G. Richter, Z. Chen, R. Fink, E. Umbach, W. Riedl, and F. Karg, J. Appl. Phys. **82**, 2411 (1997).
[6] C. Heske, R. Fink, E. Umbach, W. Riedl, and F. Karg, Appl. Phys. Lett. **68**, 3431 (1996).
[7] C. Heske, D. Eich, R. Fink, E. Umbach, S. Kakar, T. van Buuren, C. Bostedt, L.J. Terminello, M.M. Grush, T.A. Callcott, F.J. Himpsel, D.L. Ederer, R.C.C. Perera, W. Riedl, and F. Karg, Appl. Phys. Lett. **75**, 2082 (1999).
[8] P. Reinhard, B. Bissig, F. Pianezzi, E. Avancini, H. Hagendorfer, D. Keller, P. Fuchs, M. Döbeli, C. Vigo, P. Crivelli, S. Nishiwaki, S. Buecheler, and A.N. Tiwari, Chem. Mater. **27**, 5755 (2015).
[9] E. Handick, P. Reinhard, J.-H. Alsmeier, L. Köhler, F. Pianezzi, S. Krause, M. Gorgoi, E. Ikenaga, N. Koch, R.G. Wilks, S. Buecheler, A.N. Tiwari, and M. Bär, ACS Appl. Mater. Interfaces **7**, 27414 (2015).
[10] P. Pistor, D. Greiner, C.A. Kaufmann, S. Brunken, M. Gorgoi, A. Steigert, W. Calvet, I. Lauermann, R. Klenk, T. Unold, and M.-C. Lux-Steiner, Appl. Phys. Lett. **105**, 063901 (2014).
[11] P. Reinhard, F. Pianezzi, B. Bissig, A. Chirilă, P. Blösch, S. Nishiwaki, S. Buecheler, and A.N. Tiwari, IEEE J. Photovolt. **5**, 656 (2015).
[12] L.M. Mansfield, R. Noufi, C.P. Muzzillo, C. DeHart, K. Bowers, B. To, J.W. Pankow, R.C. Reedy, and K. Ramanathan, IEEE J. Photovolt. **4**, 1650 (2014).
[13] F. Pianezzi, P. Reinhard, A. Chirilă, B. Bissig, S. Nishiwaki, S. Buecheler, and A.N. Tiwari, Phys. Chem. Chem. Phys. **16**, 8843 (2014).
[14] F. Pianezzi, P. Reinhard, A. Chirilă, S. Nishiwaki, B. Bissig, S. Buecheler, and A.N. Tiwari, J. Appl. Phys. **114**, 194508 (2013).
[15] A. Laemmle, R. Wuerz, and M. Powalla, Phys. Status Solidi RRL – Rapid Res. Lett. **7**, 631 (2013).
[16] P. Jackson, D. Hariskos, R. Wuerz, O. Kiowski, A. Bauer, T.M. Friedlmeier, and M. Powalla, Phys. Status Solidi RRL – Rapid Res. Lett. **9**, 28 (2015).
[17] P. Jackson, D. Hariskos, R. Wuerz, W. Wischmann, and M. Powalla, Phys. Status Solidi RRL – Rapid Res. Lett. **8**, 219 (2014).
[18] M.A. Contreras, B. Egaas, P. Dippo, J. Webb, J. Granata, K. Ramanathan, S. Asher, A. Swartzlander, and R. Noufi, in *Conf. Rec. Twenty-Sixth IEEE Photovolt. Spec. Conf.* (1997), pp. 359–362.
[19] http://www.globalsolar.com/company/technology (accessed March 25 2017).
[20] http://www.stion.com/technology/gen-1/ (accessed March 25 2017).
[21] http://miasole.com/products/ (accessed March 25 2017).
[22] M.P. Seah, Surf. Interface Anal. **31**, 721 (2001).

[23] T. Gleim, C. Heske, E. Umbach, C. Schumacher, W. Faschinger, C. Ammon, M. Probst, and H.-P. Steinrück, Appl. Phys. Lett. **78**, 1867 (2001).
[24] L. Weinhardt, O. Fuchs, D. Groß, E. Umbach, C. Heske, N.G. Dhere, A.A. Kadam, and S.S. Kulkarni, J. Appl. Phys. **100**, 024907 (2006).
[25] NIST X-ray Photoelectron Spectroscopy (XPS) Database Main Search Menu http://srdata.nist.gov/xps/main_search_menu.aspx (accessed March 2017).
[26] M. Wojdyr, J. Appl. Crystallogr. **43**, 1126 (2010).
[27] M. Bär, S. Nishiwaki, L. Weinhardt, S. Pookpanratana, O. Fuchs, M. Blum, W. Yang, J.D. Denlinger, W.N. Shafarman, and C. Heske, Appl. Phys. Lett. **93**, 244103 (2008).